Clinopyroxene Lattice Deformations: The Roles of Chemical Substitution and Temperature[1]

Yoshikazu Ohashi,[2] and Charles W. Burnham

*Department of Geological Sciences, Harvard University,
Cambridge, Massachusetts 02138*

Abstract

The changes in unit-cell parameters associated with Ca-Fe substitution and with thermal expansion for compositions between hedenbergite and ferrosilite have been calculated using lattice parameters determined from back-reflection Weissenberg and 4-circle diffractometer measurements. Although unit cell volume increases with Ca content and temperature, the strain ellipsoids for the two effects are quite different. The largest expansion associated with adding Ca is located 50°-60° from +c toward +a in the a-c plane, whereas this is approximately the smallest thermal expansion direction. Replacement of a small atom by a large atom appears to have a significant effect on the repulsive terms associated with chemical bonds, and thus causes shorter bonds to undergo more expansion. Comparison with recently reported lattice expansions of spodumene and acmite shows that the orientation of the thermal expansion ellipsoid depends on the geometry of the M2 polyhedron.

Introduction

Papike *et al* (1972) discussed differences between chemical and thermal structural expansions in pyroxenes. Although both mechanisms cause an increase in size of the M1 octahedron, the response of the silicate chains is quite different. Because chain straightening is characteristic of thermal expansion, it was concluded that, as a first approximation, thermal expansion for pyroxenes could be considered in terms of rotation of fairly rigid polyhedral bodies with the linking oxygens acting as pivotal points.

In this study, the M1 octahedron is completely filled with Fe^{2+}; consequently the only changes observed must be due mostly to thermal effects. As a result, we will concentrate on the effects of the M2 cation on structural expansion.

In pyroxenes increasing calcium content produces the same overall effects as raising the temperature. When pigeonite is heated, its space group changes from $P2_1/c$ to $C2/c$, the space group of augite. The unit-cell volumes increase with both calcium content and temperature. In this study the detailed effects of composition and temperature on lattice deformations are compared in terms of a strain ellipsoid.

If the temperature of a crystal is changed, the bond distances and angles also change, resulting in deformation of the unit cell. In solid solutions the change of chemical composition often yields a continuous change of lattice parameters. In either case, if the degree of deformation is much smaller than the original unit-cell dimension, it can be specified by a second rank tensor (Nye, 1957, Chap. 6) that describes the transformation of a sphere in the unstrained body to an ellipsoid. In crystals with orthorhombic symmetry or higher, the principal axes of the ellipsoid (usually called a strain ellipsoid) are constrained. In this case measurements of the expansions of the lattice parameters immediately give the principal strain components. However, in the monoclinic and triclinic systems, it will usually be incomplete to represent a lattice change in terms of lattice parameter expansions instead of a strain tensor. The largest and smallest lattice expansions in the monoclinic and triclinic systems are not necessarily aligned parallel to the crystallographic axes, because the principal axes of the strain tensor ellipsoid in those crystal systems are not constrained to lie along the crystallographic axes, except that one principal axis must lie parallel to **b** in the monoclinic system. Volume expansion is given by the trace of the strain tensor based on Cartesian coordinates. Relationships between lattice parameters and strain tensor components for the triclinic crystal system are given in the Appendix.

Strain tensor components based on the Cartesian axes, $\mathbf{x}(\|\mathbf{a}^*)$, $\mathbf{y}(\|\mathbf{b})$ and $\mathbf{z}(\|\mathbf{c})$ are given by equation A-10 for the second setting of the monoclinic system. In these equations a_i, b_i, c_i and β_i are lattice parameters before ($i = 0$) and after ($i = 1$) the deformation. The ϵ_{mn}'s are thus expressed in terms of two sets of lattice parameters. Note particularly that ϵ_{13} is required in addition to ϵ_{11}, ϵ_{22}, and ϵ_{33}. An equivalent representation of the strain ellipsoid is in terms of its three principal strain components ϵ_m ($m = 1, 2, 3$) plus directions of the principal axes; these quantities are eigenvalues and eigenvectors respectively of the tensor $[\epsilon]$.

A sphere in the unstrained body

$$\mathbf{u}^2 + \mathbf{v}^2 + \mathbf{w}^2 = 1$$

becomes an ellipsoid after deformation

$$\frac{\mathbf{u}^2}{(1 + \epsilon_1)^2} + \frac{\mathbf{v}^2}{(1 + \epsilon_2)^2} + \frac{\mathbf{w}^2}{(1 + \epsilon_3)^2} = 1$$

where $\mathbf{u}$, $\mathbf{v}$, and $\mathbf{w}$ are based on unit base vectors parallel to three principal axes.

From lattice parameters listed in Table 1, principal strain components have been calculated for several clinopyroxenes (Tables 2 and 3).

Results

Lattice deformation due to changes of calcium content

A comparison of lattice parameters of clinopyroxenes with different calcium contents should reveal the effect of calcium atoms on the structure. The

TABLE 2. Principal Strain Components Due to Chemical Substitution on the Join Hedenbergite-Ferrosilite

	Principal Strain Components [x10^{-4} per 1% Fs → Wo]			Orientation of Principal Axes*		
	ϵ (max)	ϵ (med)	ϵ (min)	r_1 (max)	r_2 (med)	r_3 (min)
Fs$_{100}$Wo$_0$ → Fs$_{85}$Wo$_{15}$	13	.07	-.1	56°	b	146°
Fs$_{85}$Wo$_{15}$ → Fs$_{75}$Wo$_{25}$	8.9	-1.7	-6.7	59°	b	149°
Fs$_{75}$Wo$_{25}$ → Fs$_{65}$Wo$_{35}$	15	-2.5	-8.0	60°	b	150°
Fs$_{65}$Wo$_{35}$ → Fs$_{50}$Wo$_{50}$	6	-0.5	-1.5	55°	145°	b

*One of the principal axes is parallel to b. Angles for other principal axes are measured from +c to +a in (010). Principal strain components and orientations were calculated using equations given in Appendix.

strain ellipsoids for several pyroxenes on the hedenbergite-clinoferrosilite join are compared in Figure 1. In each case the sphere represents the lattice of the lower Ca phase and the ellipsoid represents the expansion that takes place as Ca content is increased. The eccentricity of these ellipsoids has been greatly exaggerated so the changes can be seen clearly. Neither the crystallographic $\mathbf{a}$ nor $\mathbf{c}$ axes are principal axes of the strain ellipsoids. The direction of largest expansion lies close to the bisector of the *obtuse* angle β.

To help explain the structural nature of this expansion, the $\mathbf{b}$-axis projection of the $M2$ polyhedron of clinoferrosilite is shown in Figure 2. The major structural variation along the hedenbergite-clinoferrosilite join is thought to result from the changing occupancy of the $M2$ polyhedron, which becomes more calcium rich and expands as the hedenbergite composition is approached. As shown in Figure 2, O2A and O2B have approximately the

TABLE 1. Clinopyroxenes Lattice Parameter Data*

	Temperature	a(Å)	b(Å)	c(Å)	β(deg.)	Source$^+$
Fs$_{100}$Wo$_0$	r.t.**	9.7085(8)	9.087(1)	5.2284(6)	108.432(4)	[1]
Fs$_{85}$Wo$_{15}$	r.t.	9.779(1)	9.088(1)	5.259(1)	107.39(1)	[1]
	300°C	9.814(2)	9.126(2)	5.270(2)	107.85(2)	[1]
Fs$_{75}$Wo$_{25}$	r.t.	9.781(2)	9.072(2)	5.246(2)	106.55(2)	[1]
Fs$_{65}$Wo$_{35}$	r.t.	9.8122(5)	9.0487(8)	5.2333(5)	105.336(6)	[1]
	400°C	9.854(2)	9.105(2)	5.257(2)	105.94(2)	[1]
Fs$_{50}$Wo$_{50}$	r.t.	9.8441(5)	9.0284(6)	5.2468(3)	104.802(3)	[2]
	r.t.	9.845(1)	9.024(1)	5.245(1)	104.74(1)	[3]
	400°C	9.870(1)	9.077(1)	5.258(1)	105.01(1)	[3]
Spodumene	r.t.	9.449(3)	8.386(1)	5.215(2)	110.10(2)	[4]
	300°C	9.468(1)	8.412(1)	5.224(1)	110.05(1)	[3]
	760°C	9.489(1)	8.460(1)	5.236(1)	109.88(1)	[3]
Acmite	r.t.	9.658(2)	8.795(2)	5.294(1)	107.42(2)	[4]
	400°C	9.677(1)	8.829(1)	5.298(1)	107.33(1)	[3]
	800°C	9.711(1)	8.876(1)	5.312(1)	107.29(1)	[3]

*Values in parentheses are one standard deviation, and refer to the last significant decimal.
**r.t. = room temperature.
$^+$[1] This study; [2] Veblen (1969); [3] Cameron et al (1972); [4] Clark et al (1969).

TABLE 3. Principal Thermal Expansion Coefficients for Several Clinopyroxenes

	Temperature Range	Principal Linear Thermal Expansion Coefficients x10^{-6} per 1°C			Volume Expansion Coefficient x10^{-6} per 1°C	Orientations**		
		ϵ(max)	ϵ(med)	ϵ(min)		r_1 (max)	r_2 (med)	r_3 (min)
Fs$_{85}$Wo$_{15}$	r.t. - 300°C	21	15	-10	26	139°	b	49°
Fs$_{65}$Wo$_{35}$	r.t. - 400°C	22	17	-7	32	144°	b	54°
Fs$_{50}$Wo$_{50}$	r.t. - 400°C	16	12	-1	27	b	142°	52°
Spodumene	r.t. - 300°C	11	9	6	26	b	64°	154°
	300°C-760°C	12	10	3	25	b	54°	144°
Acmite	r.t. - 400°C	10	7	2	19	b	72°	162°
	400°C-800°C	13	9	7	29	b	79°	169°

*Principal linear thermal expansion coefficients and orientations were calculated using equations given in Appendix.
**One of the principal axes is parallel to b. Angles for other principal axes are measured from +c toward +a in (010).
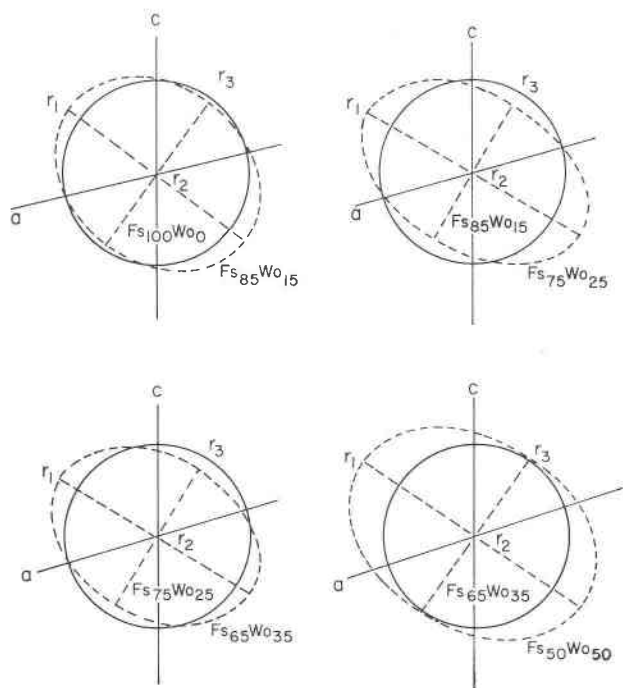
FIG. 1. Strain ellipsoids for lattice deformation from increasing Ca-content on the join hedenbergite-ferrosilite. The sphere in the lower Ca phase is considered to become the ellipsoid as Ca content is increased. The eccentricity of the ellipsoid has been exaggerated.

FIG. 2. The $M2$ polyhedron of clinoferrosilite. Note that the O2A-$M2$–O2B is the shortest O–$M2$–O path and lies in the obtuse β. The y-coordinates in percent of b are shown together with bond distances.

same y-coordinate as that of the $M2$ atom; moreover, these three atoms are almost collinear in a direction close to the bisector of the obtuse β and normal to the **b**-axis. $M2$–O2B is the shortest bond in the $M2$ polyhedra and $M2$–O2A, the second shortest. When Fe atoms are replaced by larger Ca atoms, one can expect the largest change along the shortest bonding direction O2A–$M2$–O2B.

The four crystallographically equivalent $M2$ polyhedra in one unit cell are related by the two-fold screw axis parallel to **b**, by the inversion center, and by the c-glide normal to **b**. In spite of different orientations of the $M2$ polyhedra, however, all O2A–$M2$–O2B directions are almost parallel to each other and to the largest strain direction caused by increasing Ca content (Fig. 3).

Lattice deformation due to temperature changes

As temperature increases, a lattice generally expands (or occasionally contracts) anisotropically. A similar strain ellipsoid can be constructed by comparing lattice parameters at two different temperatures.
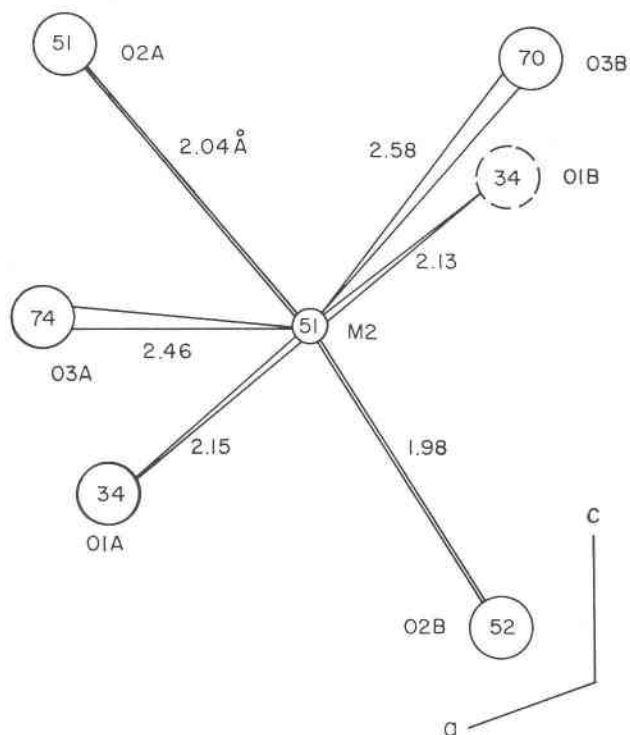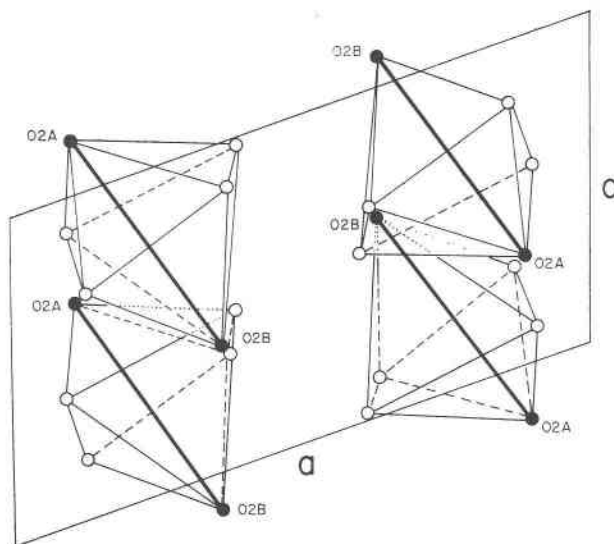

FIG. 3. Four equivalent $M2$ sites in one clinopyroxene unit cell. All O2A–$M2$–O2B directions are almost parallel in spite of different polyhedral orientations.
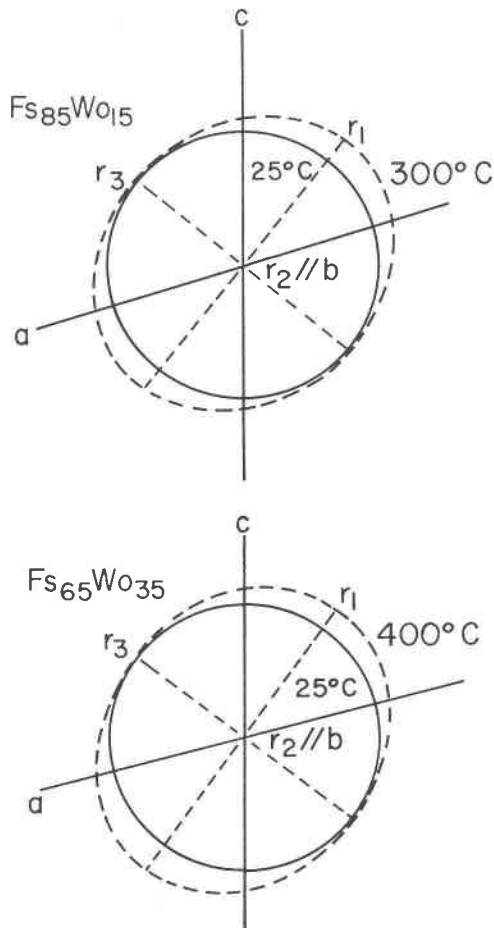
FIG. 4. Thermal expansion ellipsoids for $Fs_{85}Wo_{15}$ and $Fs_{65}Wo_{35}$. The eccentricity of the ellipsoid has been exaggerated.

Strain ellipsoids due to temperature change are shown for $Fs_{85}Wo_{15}$[3] and $Fs_{65}Wo_{35}$[3] in Figure 4. The shortest principal axis of the ellipsoid bisects the obtuse β angle. This presents a marked contrast to the Ca-replacement strain ellipsoids in which this direction corresponds to the greatest expansion.

An interpretation of the result is not as simple as that for the strain ellipsoids due to Ca, because structural changes at different temperatures involve changes of all interatomic distances (thermal expansions) and also relative rotations of these interatomic vectors. As far as the M2 site is concerned, the shortest O2A–M2–O2B direction approximately corresponds to the smallest expansion direction of the strain ellipsoid.

[3] Compositions given by mole percent of Fs = $FeSiO_3$ and Wo = $CaSiO_3$.

Comparison with thermal expansions of other pyroxenes

In clinopyroxenes on the join hedenbergite-ferrosilite the shortest M2–O bond is always M2–O2 even though the M2 coordination polyhedra vary in shape (Ohashi and Burnham, 1972). However, in some clinopyroxenes not in the standard pyroxene quadrilateral (the diopside-hedenbergite-ferrosilite-enstatite system), the shortest M2–O bond is not M2–O2. To permit comparison, the thermal expansion data for spodumene ($LiAlSi_2O_6$) and acmite ($NaFe^{3+}Si_2O_6$) (Cameron et al, 1972) have been used to calculate the strain ellipsoids shown in Figure 5. The degree of anisotropy is smaller (Table 3) and the orientations differ markedly from those in Figure 4. The largest expansion is observed along **b**, and the smallest expansion is not parallel but instead almost perpendicular to the M2–O2 direction. Unlike clinopyroxenes in the pyroxene quadrilateral (Table 4), the M2 site in spodumene and acmite is occupied by the monovalent ions, Li and Na, respectively, and the shortest M2–O bond is not M2–O2 but M2–O1 (Clark, Appleman, and Papike, 1969). Thus the differences between the thermal expansion ellipsoids in Figures 4 and 5 may be due to differences in the M2 site—the M2–O bond distances and the valences of the M2 cations.

Compressibility surface in clinopyroxenes

Linear compressibility, which is the relative change in length of a line per unit of hydrostatic pressure, in general varies with direction just as does thermal expansion. As shown in Figure 6, Kumazawa (1969) calculated the reciprocal linear compressibility surfaces for augite and acmite from the elastic constant data of Aleksandrov et al (1963). Elastically the stiffest direction, corresponding to the largest reciprocal linear compressibility, is found along the direction bisecting **a** and **c** in obtuse angle β. In augite the direction is approximately the smallest thermal expansion direction (Fig. 4). Since the chemical composition of the acmite for which the reciprocal compressibility surface was constructed is not available, there is a possibility that some of the differences between the thermal expansion data of Cameron et al (1972) and reciprocal compressibility of Kumazawa (1969) may be attributed to chemical differences.

As pointed out by Kumazawa (1969), anisotropies of linear compressibility as well as thermal expansion cannot be explained simply by the silicate
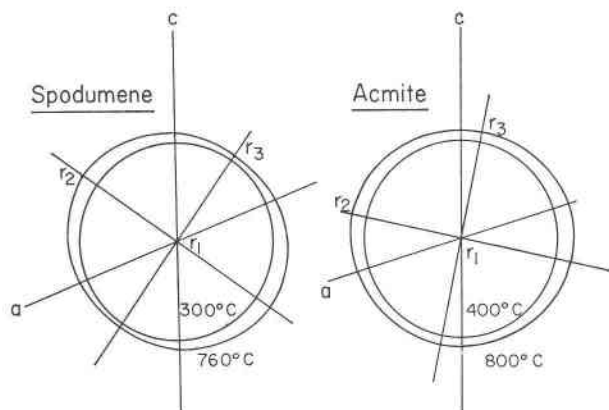
FIG. 5. Thermal expansion ellipsoids for spodumene and acmite calculated from lattice parameters determined by Cameron *et al* (1972). The smallest expansion direction is close to the direction of the largest expansion found in $Fs_{85}Wo_{15}$ and $Fs_{85}Wo_{35}$ (see Figure 4). The eccentricity of the ellipsoid has been exaggerated.

TABLE 4. Comparison of the *M2*–O Bond Distances at Room Temperature for Several Clinopyroxenes

| | Ohashi & Burnham (1972) | | Veblen (1969) | Clark et al (1969) | |
	$Fs_{85}Wo_{15}$	$Fs_{65}Wo_{35}$	$Fs_{50}Wo_{50}$	Spodumene	Acmite
M2-O1A	2.177 Å	2.300	2.358	2.105*	2.398*
O1B	2.165				
O2A	2.120	2.261*	2.342*	2.278	2.415
O2B	2.034*				
O3A	2.800	2.701	2.631	2.251	2.430
O3B	2.896				
O3A'	(3.040)	2.760	2.725	(3.144)	2.831
O3B'	2.817				

Note that the shortest M2-O bond indicated by * is the M2-O2 in clinopyroxenes of Fs-Wo compositions, but the M2-O1 in spodumene and acmite. Thermal expansion ellipsoids are different in these two groups (see Table 3 and Figures 4 and 5).

chain structure. No principal axes of these surfaces coincide in direction with the silicate chains running along **c**. This behavior reinforces the view that the structural changes produced by temperature and pressure changes are dictated in pyroxenes primarily by the response of metal-oxygen bonds to changing conditions, and not by the behavior of the silicate chains.

Appendix: Relationships between the Strain Tensor and Lattice Parameters

We now derive a relationship between lattice parameters and strain tensor components. Let us first define a strain tensor [S] in terms of lattice parameters as

$$\begin{bmatrix} s_{11} & s_{12} & s_{13} \\ s_{21} & s_{22} & s_{23} \\ s_{31} & s_{32} & s_{33} \end{bmatrix} \begin{bmatrix} \mathbf{a}_0 \\ \mathbf{b}_0 \\ \mathbf{c}_0 \end{bmatrix} = \begin{bmatrix} \mathbf{a}_1 \\ \mathbf{b}_1 \\ \mathbf{c}_1 \end{bmatrix} - \begin{bmatrix} \mathbf{a}_0 \\ \mathbf{b}_0 \\ \mathbf{c}_0 \end{bmatrix} \quad \text{(A-1)}$$

where $\mathbf{a}_i$, $\mathbf{b}_i$ and $\mathbf{c}_i$ are direct lattice vectors before ($i = 0$) and after ($i = 1$) a deformation. Using matrix and column vector notations, (A-1) is in short

$$\mathbf{S} \cdot \mathbf{a}_0 = \mathbf{a}_1 - \mathbf{a}_0 \quad \text{(A-1')}$$

Postmultiplying (A-1') by the reciprocal row vector $\tilde{\mathbf{a}}_0^* = (\mathbf{a}_0^* \mathbf{b}_0^* \mathbf{c}_0^*)$, we obtain

$$\mathbf{S} \cdot \mathbf{a}_0 \cdot \tilde{\mathbf{a}}_0^* = \mathbf{S} = \mathbf{a}_1 \cdot \tilde{\mathbf{a}}_0^* - \mathbf{I} \quad \text{(A-2)}$$

where **I** is a 3 × 3 unit matrix. For crystal systems

other than triclinic, certain relations between vectors $[\mathbf{a}_0^* \mathbf{b}_0^* \mathbf{c}_0^*]$ and $[\mathbf{a}_1 \mathbf{b}_1 \mathbf{c}_1]$ exist. For example, $\mathbf{a}_1 \cdot \mathbf{b}_0^* = \mathbf{c}_1 \cdot \mathbf{b}_0^* = 0$, $\mathbf{b}_1 \cdot \mathbf{b}_0^* = |\mathbf{b}_1| \, |\mathbf{b}_0^*| = b_1/b_0$ for the 2nd setting of the monoclinic system. Note that in general $\mathbf{a}_1 \cdot \mathbf{c}_0^* \neq 0$ because of changes in β.

Unless a fixed coordinate system is established outside a crystal (*e.g.*, the instrumental axes of a single-crystal diffractometer), information on angular relations between the $\mathbf{a}_1$ and $\mathbf{a}_0^*$ cells cannot be obtained. However, if we exclude *pure* rotations as not being of interest (which is usually done in a strain tensor analysis) we can calculate a symmetric strain tensor from two sets of lattice parameters as shown below.

Let us define unit base vectors **x**, **y** and **z** of the Cartesian system such that **z** is parallel to **c**, **x** parallel
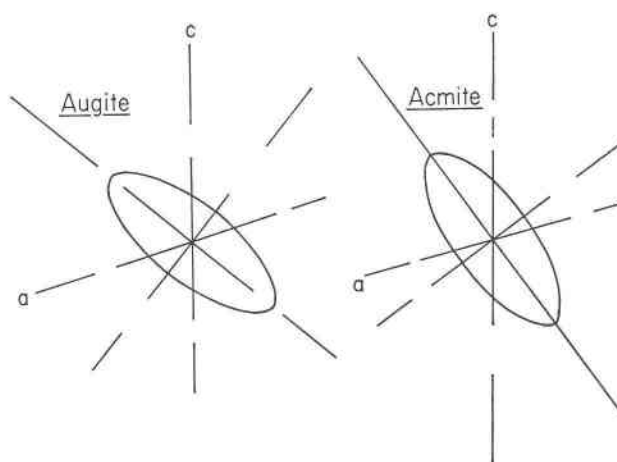

FIG. 6. Reciprocal linear compressibility surfaces in pyroxenes (after Kumazawa, 1969). The intermediate axis is parallel to **b**. The stiffest direction, corresponding to the largest reciprocal linear compressibility, is found in the obtuse β angle.

to $\mathbf{a}^*$ and $\mathbf{y} = \mathbf{z} \times \mathbf{x}$. Then the lattice vectors are expressed in terms of $\mathbf{x}$, $\mathbf{y}$, and $\mathbf{z}$ as

$$\mathbf{a}_i = \mathbf{Q}_i \mathbf{x}_i \qquad (i = 0, 1) \tag{A-3}$$

the transformation matrix $\mathbf{Q}_i$ is given by

$$\mathbf{Q}_i = \begin{vmatrix} \dfrac{a_i p_i}{\sin \alpha_i} & \dfrac{a_i(\cos \gamma_i - \cos \alpha_i \cos \beta_i)}{\sin \alpha_i} & a_i \cos \beta_i \\ 0 & b_i \sin \alpha_i & b_i \cos \alpha_i \\ 0 & 0 & c_i \end{vmatrix} \tag{A-4}$$

where

$$p_i = (1 - \cos^2 \alpha_i - \cos^2 \beta_i - \cos^2 \gamma_i$$
$$+ 2 \cos \alpha_i \cos \beta_i \cos \gamma_i)^{1/2}$$

The reciprocal lattice vectors are given by

$$\mathbf{a}_i^* = \tilde{\mathbf{Q}}_i^{-1}\mathbf{x}_i^* = \tilde{\mathbf{Q}}_i^{-1}\mathbf{x}_i \qquad (\mathbf{x}_i = \mathbf{x}_i^*) \tag{A-5}$$

Let $\mathbf{R}$ be a transformation matrix from the $\mathbf{x}_0$ system to the $\mathbf{x}_1$ system,

$$\mathbf{x}_1 = \mathbf{R}\mathbf{x}_0 \tag{A-6}$$

Since both $\mathbf{x}_0$ and $\mathbf{x}_1$ are the base vectors of the (right-handed) Cartesian coordinates, $\mathbf{R}$ represents a pure rotation operation.

Substituting (A-3), (A-5) and (A-6) into (A-2), we have

$$\mathbf{S} = \mathbf{Q}_1\mathbf{x}_1(\widetilde{\tilde{\mathbf{Q}}_0^{-1}\mathbf{x}_0}) - \mathbf{I}$$
$$= \mathbf{Q}_1\mathbf{R}\mathbf{x}_0\tilde{\mathbf{x}}_0\mathbf{Q}_0^{-1} - \mathbf{I}$$
$$= \mathbf{Q}_1\mathbf{R}\mathbf{Q}_0^{-1} - \mathbf{I} \tag{A-7}$$

By a similarity transformation the tensor [S] based on the crystallographic axes is transformed to the tensor [E] based on the Cartesian system $\mathbf{x}_1$.

$$\mathbf{E} = \mathbf{Q}_0^{-1}\mathbf{S}\mathbf{Q}_0 = \mathbf{Q}_0^{-1}[\mathbf{Q}_1\mathbf{R}\mathbf{Q}_0^{-1} - \mathbf{I}]\mathbf{Q}_0$$
$$= \mathbf{Q}_0^{-1}\mathbf{Q}_1\mathbf{R} - \mathbf{I} \tag{A-8}$$

If we exclude a pure rotation $\mathbf{R}$, the *asymmetric* tensor is $\mathbf{E}_R = \mathbf{Q}_0^{-1}\mathbf{Q}_1 - \mathbf{I}$ and then a *symmetric* strain tensor [ε] can be defined by

$$\boldsymbol{\varepsilon} = \tfrac{1}{2}(\mathbf{E}_R + \tilde{\mathbf{E}}_R)$$
$$= \tfrac{1}{2}(\mathbf{Q}_0^{-1}\mathbf{Q}_1 + \widetilde{\mathbf{Q}_0^{-1}\mathbf{Q}_1}) - \mathbf{I} \tag{A-9}$$

Putting observed lattice parameters into (A-4) we can evaluate $\mathbf{Q}_0$ and $\mathbf{Q}_1$ for lattices before and after the deformation. From these $\mathbf{Q}_0$ and $\mathbf{Q}_1$ the strain tensor [ε] can be calculated with (A-9).

For the 2nd monoclinic setting, $\mathbf{Q}_0^{-1}$ and $\mathbf{Q}_1$ are

$$\mathbf{Q}_0^{-1} = \begin{vmatrix} 1/(a_0 \sin \beta_0) & 0 & -\cos \beta_0/(c_0 \sin \beta_0) \\ 0 & 1/b_0 & 0 \\ 0 & 0 & 1/c_0 \end{vmatrix}$$

$$\mathbf{Q}_1 = \begin{vmatrix} a_1 \sin \beta_1 & 0 & a_1 \cos \beta_1 \\ 0 & b_1 & 0 \\ 0 & 0 & c_1 \end{vmatrix}$$

Components of the tensor [ε] are given by

$$\left. \begin{aligned} \epsilon_{11} &= \frac{a_1 \sin \beta_1}{a_0 \sin \beta_0} - 1 \\ \epsilon_{22} &= \frac{b_1}{b_0} - 1 \\ \epsilon_{33} &= \frac{c_1}{c_0} - 1 \\ \epsilon_{13} &= \epsilon_{31} = 1/2\left(\frac{a_1 \cos \beta_1}{a_0 \sin \beta_0} - \frac{c_1 \cos \beta_0}{c_0 \sin \beta_0}\right) \\ \epsilon_{12} &= \epsilon_{23} = 0 \end{aligned} \right\} \tag{A-10}$$

The principal strain components and their directions are given by the eigenvalues and the eigenvectors of the tensor [ε]. For the case under concern

$$\begin{vmatrix} \epsilon_{11} & 0 & \epsilon_{13} \\ 0 & \epsilon_{22} & 0 \\ \epsilon_{13} & 0 & \epsilon_{33} \end{vmatrix}$$

becomes

$$\begin{vmatrix} \epsilon_1 & 0 & 0 \\ 0 & \epsilon_2 & 0 \\ 0 & 0 & \epsilon_3 \end{vmatrix}$$

when the base vectors are transformed to the principal axes. The principal components are given by

$$\left. \begin{aligned} \epsilon_2 &= \epsilon_{22} \\ \epsilon_1, \epsilon_3 &= \tfrac{1}{2}(\epsilon_{11} + \epsilon_{33} \pm \sqrt{D}) \end{aligned} \right\} \tag{A-11}$$

where $+$ and $-$ correspond to ϵ_1 and ϵ_3 respectively and

$$D = (\epsilon_{11} + \epsilon_{33})^2 + 4(\epsilon_{13}^2 - \epsilon_{11}\epsilon_{33}) \tag{A-12}$$

By symmetry the ϵ_2-axis is parallel to the **b**-axis. The ϵ_1-axis is normal to **b** and makes an angle θ with **c**.

$$\theta = \tan^{-1}\left(\frac{\epsilon_{13}}{\epsilon_1 - \epsilon_{11}}\right) \tag{A-13}$$

where positive θ is measured toward the $+\mathbf{a}$-axis.

Acknowledgments

References

ALEKSANDROV, K. S., T. V. RYZHOVA, AND B. P. BELIKOV (1963) The elastic properties of pyroxenes. *Kristallografiya,* **8,** 738–741 [English trans. *Soviet Phys. Crystallogr.,* **8,** 589–591.]

CAMERON, M., S. SUENO, AND J. J. PAPIKE (1972) High-temperature crystal chemistry of acmite, hedenbergite, and spodumene (abstr). *Geol. Soc. Amer. Abstr. Programs,* **4,** 466.

CLARK, J. R., D. E. APPLEMAN, AND J. J. PAPIKE (1969) Crystal-chemical characterization of clinopyroxenes based on eight new structure refinements. *Mineral. Soc. Amer. Spec. Pap.* **2,** 31–50.

KUMAZAWA, M. (1969) The elastic constants of single-crystal orthopyroxene. *J. Geophys. Res.* **74,** 5973–5980.

NYE, J. F. (1957) *Physical properties of crystals.* Oxford University Press, London.

OHASHI, Y., AND C. W. BURNHAM (1972) Clinopyroxene crystal structures on the join hedenbergite-ferrosilite at 25°C and 400°C (abstr). *Geol. Soc. Amer. Abstr. Programs,* **4,** 617.

PAPIKE, J. J., C. T. PREWITT, S. SUENO, AND M. CAMERON (1972) Pyroxenes: Comparison of chemical and thermal structural expansion. *Trans. Amer. Geophys. Union,* **53,** 545.

VEBLEN, D. R. (1969) *The crystal structures of hedenbergite and ferrosilite.* A.B. Thesis, Department of Geological Sciences, Harvard University.